Flows Characteristics of Two Immiscible Swirling Fluids in a Cylinder

Kenza BRAHMA*, Rachid SACI**, Kacem MANSOURI*, Malika IMOULA**

*Laboratory of Energy, Mechanical and Engineering "LEMI", Faculty of Technology, University M'hamed Bougara of Boumerdes, Independence Avenue, Boumerdes 35 000, Algeria, E-mail: k.brahma@univ-boumerdes.dz

**Dynamic of Engines and Vibroacoustic Laboratory, Faculty of Technology, University M'hamed Bougara of Boumerdes, Independence Avenue, Boumerdes 35 000, Algeria, E-mail: r.saci@univ-boumerdes.dz

1. Introduction

Swirling flows of immiscible Newtonian fluids have attracted a great deal of interest as they possess a variety of distinctive characteristics, not observed in single fluid flows[1, 2]. The class of air-water flows driven by one end wall of a disk-cylinder system motivated numerous studies as they provide well controlled low stress environment and efficient mixing required for tissue growth in aerial bioreactors [3, 4, 5]. Of note, experiments carried out on flows driven by the disk rotation adjacent to the water phase revealed the occurrence of on-axis bubble breakdown, evolving into a ring type vortex with increasing rotation rate [6]. Numerical simulations, based on free-stress interface models, confirmed qualitatively the findings but failed to capture the observed interface deformation and related eddies [7]. The transition from bubble to toroidal vortices, associated to highly deformed interface was predicted numerically under the effect of reducing water volume fraction [8]. Model flows driven by the disk adjacent to the air phase were shown to display substantial upward interface deformation, induced by the competition of the circulations that develop at and either side of the interface [9]. In the same set up, creeping flows were found to exhibit multicellular topology as a result of the small air to water density ratio involved.

Experiments involving helical flows of liquid-liquid systems were also widely used; for instance, that carried out by using silicone oil-water [10, 11], characterized by large viscosity and small density differences. In axisymmetric flow parameter regimes and strong advection of angular momentum, results revealed significant enlargement of the interface area associated to drastic changes of the interface topology; including striking dome like forms that evolve into bell shapes upon increasing either the rotation rate or the oil phase volume fraction.

The role of individual physical fluids properties as well as that of the associated parameters which control the flow topology of a two-fluid system in a cylinder were studied numerically [12]. The findings demonstrated that the dynamics of the interface is determined by the balance between the coupling action of viscous stresses, inertia and surface tension. Tsai et al. [13] employed soybean oil-water and reported, on the basis of varying lid rotation rate and oil fluid volume fraction, that the interface is connected to the vortex breakdown phenomenon. More recent PIV experiments [14] adopted a two-fluid layer such that the kinematic viscosity of the fluid adjacent to the rotating lid is much higher (9 times) than that of the lighter fluid. With increasing rotation rate, breakdown was shown to occur almost simultaneously in both fluids while the swirling flows remained steady and axisymmetric.

Different scenarios may be observed in the case of two immiscible Newtonian fluids filling a cylindrical cavity with an immersed rotating central rod as first evidenced experimentally by Bonn et al. [1]. Upon increasing the rod rotation rate, the authors observed the occurrence of Taylor type vortices along the rod part adjacent to the less viscous fluid, associated to a rod climbing like effect of the interface. This rather surprising phenomenon, unlike its counterpart that characterizes non Newtonian viscoelastic fluids, is at-tributed to the centrifugal instability that generates the eddies structure and controls the interface orientation according to the viscosity ratio as reported later by Zhao et al. [5] on the basis PIV measurements, qualitatively supported by numerical simulations despite major discrepancies. More recently, Chandra et al. [15] addressed the role of the interfacerod contact angle modeling by associating PIV measurements into the numerical method which led to considerable mismatch reduction between experiments and numerical simulations.

The experimental characterization of the interface dynamics is a very difficult and chalanging task to carry out and capture accurately, even under well controlled operating conditions, due to the eddies scales and sensitivity involved [2, 16, 17, 19]. This motivated the current numerical study to explore the helical flows of a two-fluid system in a cylinder; aiming at providing detailed quantitative characteristics, over a wide range of parameters, that highlight the conditions of flow stagnation and the sensitivity of the associated eddies structure to the distinct and combined effect of back-ground rotation rates and fluids volume fraction. The findings are of fundamental interest and provide guidance for future investigations that span parameter regimes involved in practical applications; for instance, the emulsification process produced by the breakup of highly sheared interfaces, the interface transport phenomena in biological reactors and interface mixing in chemical industry [3, 4, 5].

The manuscript is arranged as follows. The problem formulation that identifies the main parameters, the numerical method of solution and validation are described in sections 2 and 3 respectively. Section 4 is devoted to the results and discussion on vortex flows driven by a single disk under effect of sidewall differential rotation. Section 5 focuses on the configuration with rotating rod-disk. Finally, a conclusion summarizes the findings.

2. Problem Description and Formulation

A vertical cylinder of height H and radius R, with a thin rod of radius R_r $(0 \leq R_r / R \leq 0.12)$ mounted at its
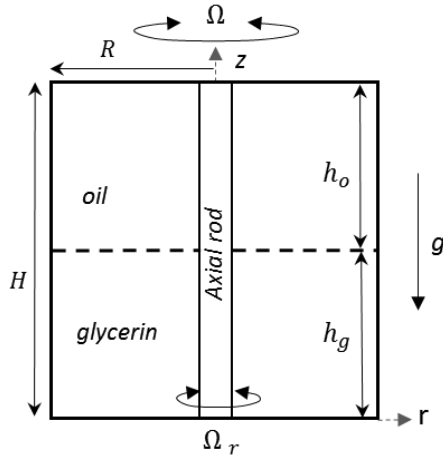
Fig. 1 Schematic of the configuration in the meridian plane

axis, is filled with two superposed immiscible Newtonian fluids as sketched in Fig. 1. The cavity lid, sidewall and rod may rotate independently at constant angular velocities Ω, Ω_S and Ω_r respectively.

At rest, the interface is flat and located at $z = h_g / R$. The fluids are individually incompressible and characterized by the density and dynamic viscosity ratios $\rho_g / \rho_o \approx 1.3$ and $\mu_o / \mu_g \approx 0.97$, where subscripts "g" and "o" refer to bottom (glycerin) and top (oil) fluids quantities respectively; chosen for the sake of comparison with prior works. In the current work, the interfacial surface tension coefficient $\sigma = 0.0315$ N/m, the material properties ratios are kept invariant and the variation of the kinematic conditions are the main focus.

Using R and $1 / \Omega$ as a length and time scales respectively, the axisymmetric flows under consideration may conveniently described by following selected non dimensional main independent parameters; namely, the rotational Reynolds number Re which drives the swirl strength of the basic state generated by the cavity lid, the rod rotational Reynolds number Re_r, the sidewall-lid rotation rate ratio S, the oil phase volume fraction Λ_o, the cavity aspect ratio Λ and the rod radius ratio δ_r defined respectively in Table 1.

Table 1
Dimentienless parameters of the problem

Rotational Reynolds number	$Re = \dfrac{\Omega R^2}{\upsilon_o}$	Oil phase volume fraction	$\Lambda_o = \dfrac{h_o}{H}$
Rod rotational Reynolds number	$Re_r = \dfrac{\Omega_r R_r^2}{\upsilon_g}$	Cavity aspect ratio	$\Lambda = \dfrac{H}{R}$
Sidewall-lid rotation rate ratio	$S = \dfrac{\Omega_S}{\Omega}$	Rod radius ratio	$\delta_r = \dfrac{R_r}{R}$

Here, υ_o and υ_g denote the kinematic viscosity coefficients of the oil and glycerin phases respectively. The axisymmetry condition reduces the description of the flows under consideration to the meridian plane (r, z) where $0 \leq r \leq 1$ and $0 \leq z \leq \Lambda$. All variables and flow fields are expressed in dimensionless form.

The 3D non-dimensional velocity field (scaled with respect to ΩR) may be expressed in terms of the stream function $\psi(r, z)$ (scale: ΩR^3) and circulation $\Gamma = vr$

(scale: ΩR^2) in order to provide an interpretation of the local meridian flow direction when necessary

$$(u, v, w) = \left(\frac{1}{r} \frac{\partial \psi}{\partial z}, \frac{\Gamma}{r}, \frac{1}{r} \frac{\partial \psi}{\partial r} \right).$$

2.1. Initial and boundary conditions

Initially, both confined fluids and walls are at rest; forming a flat interface. At $t = 0$, the cavity lid is set to rotate impulsively to a uniform angular velocity. Boundary conditions which apply for all times $(0 \leq t \leq t_f)$; t_f being the prescribed final time which depends on the configuration:

- No slip conditions at all (stationary and rotating) walls and symmetry (regularity) condition is assumed at the cavity axis (cavity without rod).

- At the fluids interface, continuity is applied for all velocity and stress components.

- Interface tracking is carried out by using the transport equation for the selected cell glycerin phase volume fraction α_g:

$$\frac{\partial \alpha_g}{\partial t} + \nabla.\left(\alpha_g \vec{v} \right) = 0, \ \left(0 \prec \alpha_g \prec 1 \right). \tag{1}$$

This is solved in conjunction with the set of mass and momentum conservation equations for each fluid that account for gravity and capillary forces [18]. These latter, in the current case of constant surface tension coefficient σ may be modeled by the continuous surface force $F_\sigma = \sigma \kappa \delta_D$ where δ_D is the Dirac distribution at the interface and $\kappa = -\nabla.(\eta_s)$ the interface local curvature oriented by the unit normal vector $\eta_s = -\nabla \alpha_g / |\nabla \alpha_g|$.

3. Method of Solution and Validation

The flows under consideration are explored by means of the code ANSYS FLUENT. A pressure-based (segregated) finite volume solver is used to solve the nonlinear transient momentum and continuity equations in both lower and upper bulk fluid domains. To resolve the interface tracking and associated dynamics, the Eulerian fixed grid volume of Fluid (VoF) model is adopted [18] in conjunction with high resolution geo-reconstruction scheme. Spatial discretization is performed by using a second order upwind scheme for both momentum and swirl velocity, PRESTO scheme is adopted for the pressure and PISO algorithm is employed for pressure-velocity coupling.

In order to assess the reliability of the above numerical approach and accuracy of the associated schemes, initial calculations were performed and applied to selected recent prior configurations for comparison [11, 14].

In Fig. 2, the steady meridian flow patterns driven by the bottom disk of a cylinder filled with two superposed immiscible fluids is shown numerically to exhibit two distinct on-axis vortex breakdown (VB) at $Re = 750$ for both the closed and open cavity; the first bubble onset being apparent in the upper (lower) fluid of the free (rigid) surface configuration. The current predicted flow topology of Fig. 2 confirms recent experimental findings [14]; in particular, the flow stagnation points locations and associated vortex type and size are in good qualitative accord.
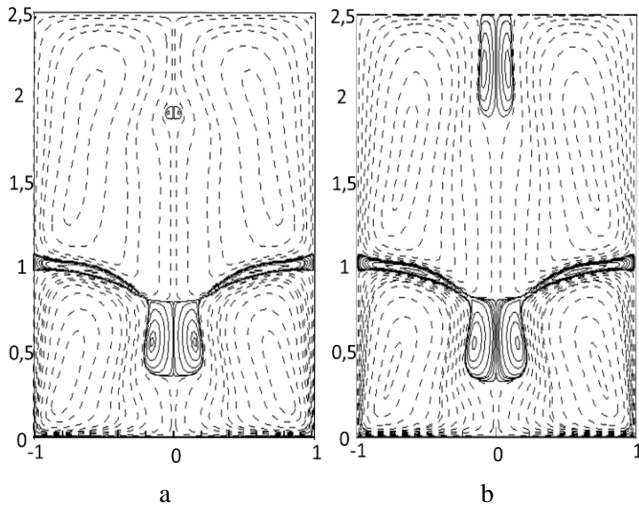
Fig. 2 Vortex breakdown onset in both phases of a two-fluid system filling a closed (a) and open (b) cavity with rotating bottom at $Re = 750$; both predicted patterns are in qualitative agreement with prior experiments [14]
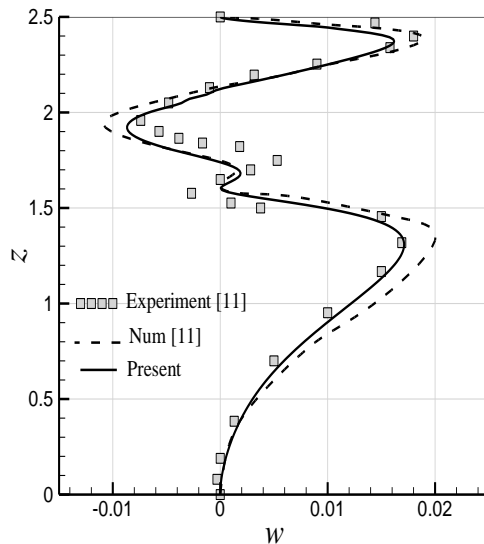

Fig. 3 Comparison of the velocity distribution along the axis of an oil-water system driven in a cylinder with rotating top; $Re = 750$, $\Lambda_o = 0.4$ (at rest $z = 1.5$)

Besides, breakdown onset in the closed cavity was found to occur at approximately $Re = 500$ which is reasonably close to the threshold value $Re = 538$ provided experimentally [14].

In addition, Fig. 3 illustrates the velocity distribution of a two-fluid flow driven by the lid rotation of a cylinder, obtained by the current simulation and that reported in a recent experimental and numerical study [11]. Very good quantitative comparison is remarked away from the interface vicinity and qualitatively, the predicted local trend within the interface region may be considered reasonable as regards to the inevitable imperfections of the experimental set up and associated operating conditions, on one hand, and the lack of physically rigorous modelling of the interface conditions, on the other hand [11; 16].

Appropriate time and space mesh grids were chosen on the basis of numerous numerical experiments to ensure convergence and constancy of the solutions. In particular, grid refinement was applied to cover and focus onto the core flow and interface regions where significant flow alterations are expected to occur. Besides, it was found efficient to use convergent solutions obtained for given Re and/or Re_r as starting conditions to explore new configurations for higher parameters values.

For instance, the selected flow topology that exhibits breakdown in both phases, used above for validation, at $(Re; z; \Lambda) = (750; 1; 2.5)$ required a mesh grid of $(n_r, n_z) = (300 \times 300)$ and an estimated initial dimensionless time step $\delta t = 0.0005$ to capture the transient behaviour before it is relaxed as the solution proceeded with increasing time. The corresponding scale residuals below which no significant changes were remarked in the solution are estimated to 10^{-4} for mass conservation and for 10^{-5} the velocity field and swirl equation.

4. Results and Discussion

4.1. Configuration without rod

4.1.1. Basic state

In the absence of the central rod, it is well established that the two-layer fluid flow driven by the low rotation rate of the cavity lid to a low constant angular velocity ($Re \leq 510$) exhibits a single large meridian clockwise (anticlockwise) circulation above (below) the interface which superimposes to the primary rotational motion. The circulation adjacent to the rotating disk is characterized by an outward spiraling flow at the lid, induced by the no slip conditions, that deviates downwards along the sidewall up to the interface, while the bulk flow is directed upwards by the Ekman suction. At the interface, an inward swirling motion takes place whose strength and radial extent depend upon the lid rotation rate as well as the coupling effect of viscous shear and surface tension. Via the interface layer, the lower less viscous fluid is consequently entrained into an inward circulatory motion which deviates downwards as a weak helical core flow before it spirals outwards at the bottom still disk and eventually forms the lower meridian circulation.

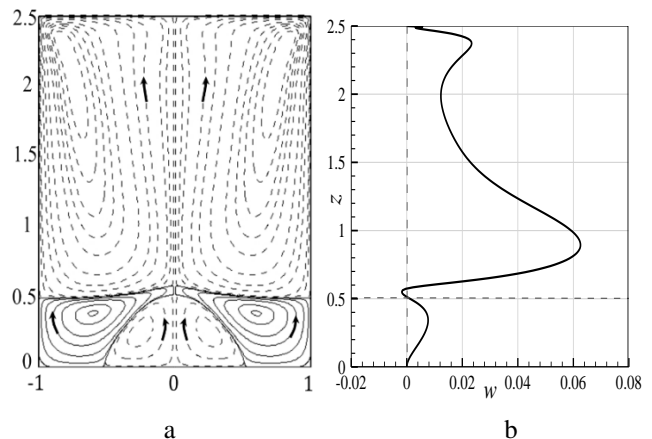Upon increasing Re, results revealed a slight interface elevation associated to the development of a

Fig. 4 Flow pattern in the meridian plane $[-1, 1] \times [0, \Lambda]$ (a), velocity distribution at the cavity axis (b) at $\Lambda_o = 0.8$ ($z = 0.5$ at rest), $Re = 1000$

secondary clockwise circulation that merges at the bottom disk center and expands with increasing rotation rate as depicted in Fig. 4, a, at the selected parameters $Re = 1000$, $\Lambda_o = 0.8$ (at rest $z = 0.5$); the corresponding meridian flows direction being schematically indicated. The velocity distribution at the cavity axis (Fig. 4, b), corresponding to this cell structure, clearly shows a modified axial flow direction and its strength either side of the interface (the maximum velocity magnitude is approximately seven times higher in the fluid adjacent to the rotating lid).

4.1.2. Effect of fluids volume fraction

This section focuses on the interface behavior and associated vortex patterns that are likely to develop, under the coupling effect of viscous shear and surface tension, when altering the fluids volume fraction over the selected range $0.2 \leq \Lambda_o \leq 0.8$ (corresponding to interface axial location (at rest $0.5 \leq z \leq 2$); the cavity aspect ratio $\Lambda = 2.5$ and the viscosity ratio $\mu_o / \mu_g \approx 0.97$ are kept invariant throughout.

Numerical predictions revealed that a decrease of the upper oil-phase volume fraction strengthens the dynamics of the interface layer and alters considerably the flow topology. This is best viewed with reference to the basic state described above and to Fig. 5 which depicts respectively the meridian streamlines over the entire meridian domain $[-1, 1] \times [0, \Lambda]$ as well as a close up of the main region of interest that focuses on the interface vicinity $[-1, 1] \times [0.5, 2.2]$, for three distinct values of the oil phase volume fraction selected over the range $0.28 \leq \Lambda_o \leq 0.68$.

The flow structure obtained at $Re = 1000$ and $\Lambda_o = 0.68$ (Fig. 5, a), compared to that shown in Fig. 4, clearly displays the emergence of an on-axis bubble type breakdown in the upper more viscous fluid, associated to a significant increase of the interface displacement within the axial core flow. The breakdown onset results from the increased angular momentum transfer which strengthens the local swirl and enhances the development of an adverse pressure gradient within the upper helical core flow [20]. This latter eventually breaks, giving rise to the bubble type reverse flow region bounded by two on-axis stagnation points schematically denoted by (1) and (2) in the corresponding close up figure. The onset conditions of flow stagnation and breakdown occurrence depend in general on the cavity aspect ratio, rotation rate, fluids volume fraction as well as the physical fluids properties; namely, the density and viscosity ratios. Compared to the pattern of Fig. 4, the oil phase reduction has also caused a considerable expansion of the circulation adjacent to the still disk and a significant shrink of the initially ambient anticlockwise circulation which evolves into an interface layer cell that extends from the sidewall to the cavity axis with a steep thickness reduction. The interface meets the cavity axis at the saddle point (0) as indicated in Fig. 5, b, (close up of the region $[-1, 1] \times [0.5, 2.2]$). Upon decreasing the fluid volume fraction to $\Lambda_o = 0.56$ (at rest, $z = 1.1$), calculations (not shown here for the sake of brevity) revealed a simultaneous increase of the interface height and bubble downward expansion that caused the coalescence of stagnation points (1) and (0) at approximately $z = 1.35$. Beyond this latter threshold parameter value, the bubble evolves into a

toroidal type vortex structure, characterized by an upstream stagnation circle which intersects the (r, z) plane at points (3) and (4) schematically illustrated in Fig. 5, c, at the selected $Re = 1000$ and $\Lambda_o = 0.44$. It is remarked that the stagnation point location (2) downstream the bubble remains located at the axis. Further decrease of the volume fraction caused the collapse of the breakdown region associated to a significant interface level increase; leading to a
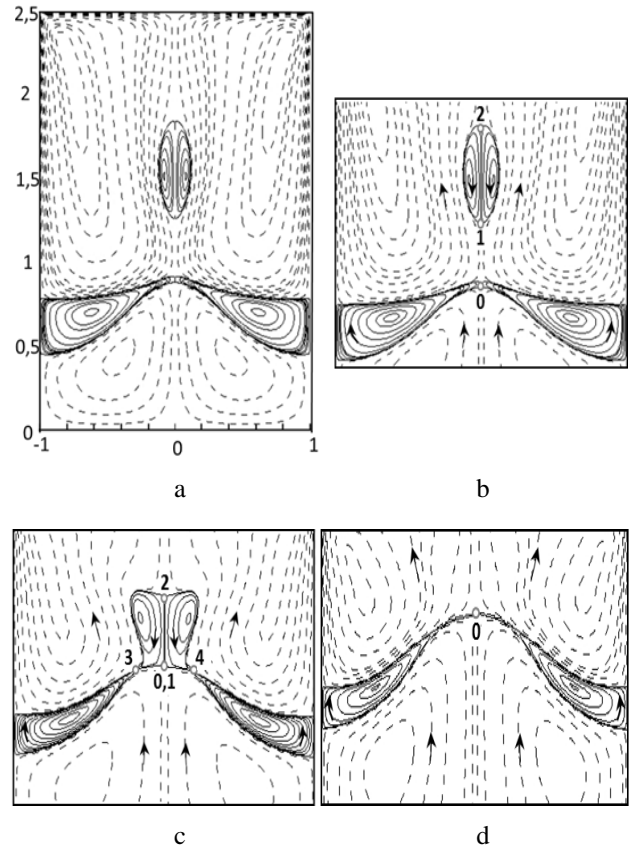

a   b

c   d

Fig. 5 Meridian flow pattern at $Re = 1000$ for three oil phase volume fraction Λ_o: a – in the entire domain $[-1, 1] \times [0, \Lambda]$ at $\Lambda_o = 0.68$ ($z = 0.8$), b – close up at $\Lambda_o = 0.68$ ($z = 0.8$), c – close up at $\Lambda_o = 0.44$ ($z = 1.4$), d – close up at $\Lambda_o = 0.28$ ($z = 1.8$)
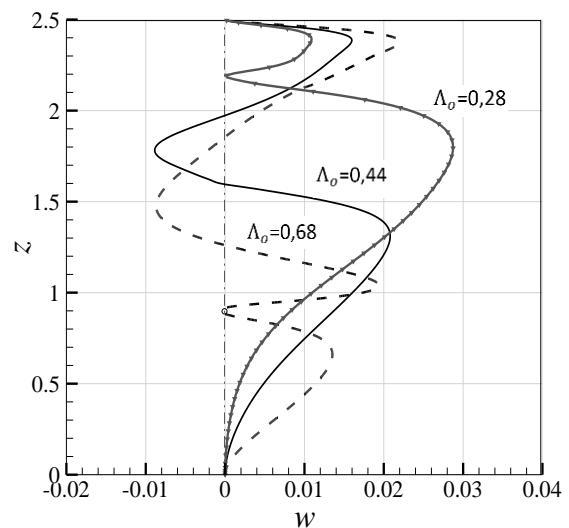

Fig. 6 Velocity distribution at the cavity axis with decreasing oil phase volume fraction, $Re = 1000$
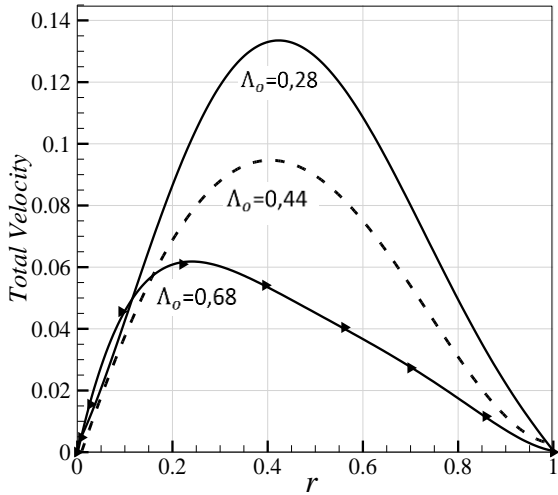
Fig. 7 Interface velocity distribution with decreasing fluid volume fraction; $Re = 1000$

bell shaped interface structure characterized by a thin but robust secondary cell as shown in Fig. 5, d, at $\Lambda_o = 0.28$. The stagnation points evolution and axial flux strength that result from the oil phase volume fraction reduction discussed above is illustrated in Fig. 6 which depicts the axial velocity distribution at the cavity axis; confirming the suppression of the axial reverse flow region ($w > 0$ for all z) with decreasing Λ_o. Fig. 7 indicate how the corresponding totale velocity at the interface intensifies (up to approximately 20%) with decreasing Λ_o.

4.1.3. Combined effect of parameters (Re, Λ_o)

Numerous numerical calculations have been carried out, by varying individually (independently) the lid rotation rate and the fluids volume fraction, which led to the establishment of the state diagram illustrated in Fig. 8. The selected parameters are considered over the ranges $500 \leq Re \leq 1100$ and $0.2 \leq \Lambda_o \leq 0.8$, for which the flows under consideration evolve into steady axisymmetric patterns.

Results focus on the onset and suppression of the distinct vortex patterns discussed in the previous section; schematically represented in the diagram. This latter clearly identifies the regions of their existence within bounding curves drawn on the basis of calculated threshold parameter values at which they appear/disappear. Over the considered range of parameters, it is observed that the threshold Re for VB onset decreases almost linearly with decreasing oil phase volume fraction as depicted by the right bounding curve of Fig.8. Also, the bounded region of breakdown occurrence widens with increasing Re. Besides, prior to its elimination and for intermediate parameter values, the diagram illustrates the existence of an inner bounded region within which the bubble evolves into a toroidal vortex structure as discussed in the previous section. This inner region, unlike the ambient one, remains approximately invariant with increasing either of the parameters. Similar scenario is remarked from the state diagram when increasing the lid rotate rate while maintaining the fluid volume fraction fixed. It is worth noting that the particular case $\Lambda_o = 0.4$ ($z = 1.5$) is very consistent with experimental observations [18].
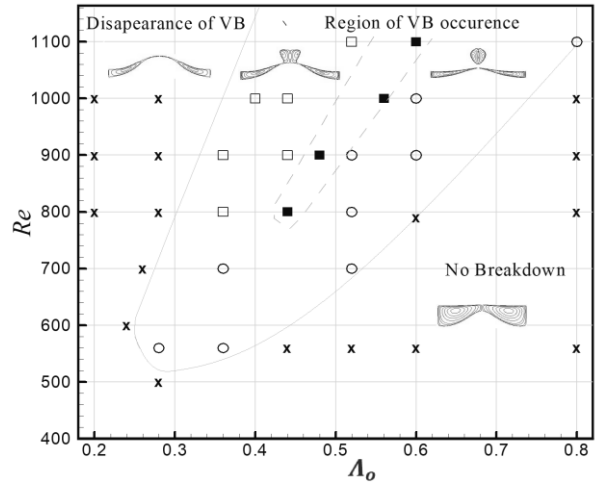

Fig. 8 (Re, Λ_o) diagram, mapping regions of bubble breakdown (VB: ○), toroidal vortex (□), interface cell structure (■) and region that lacks breakdown (x)

4.1.4. Selected vortex characteristics

The secondary flows under consideration result from the interface behaviour and associated reverse flows either side of the interface, and may be characterized by the type and location of the corresponding stagnation points/circles.

In this section interest is focused on the vortex characteristics that develop under the variation of the lid rotation rate. Fig. 9 provides, with increasing Re, selected stagnation flow characteristics of a prototype model flow that exhibits a vortex bubble associated to an interface cell structure. It is remarked that, over the approximate initial range $400 < Re < 540$, the flow lacks breakdown and the interface level undergoes a slight increase ($< 4\%$). Further increase of Re causes the bubble to expand axially (about 6 times its initial length) with its downstream (upstream) stagnation point moving slightly upward (downward). Simultaneously, the associated interface level also increases (almost linearly) until it coincides with that of the bubble as illustrated by the intersection of the corresponding curves at approximately $Re = 800$.Consequently, beyond this latter Re limit, the bubble bifurcates into a toroidal
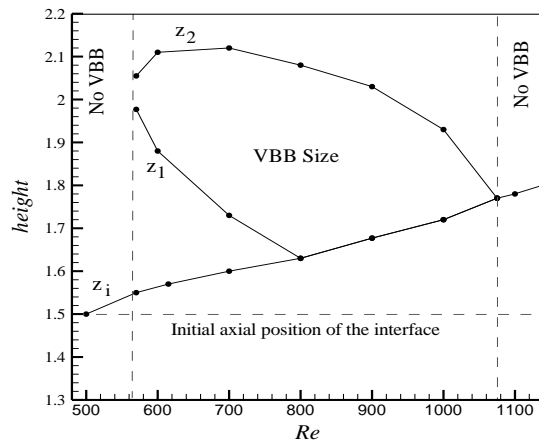

Fig. 9 Diagram illustrating the interface height z_i and vortex breakdown bubble (VBB) onset and evolution at the cavity axis with increasing Re at $\Lambda_o = 0.4$ z_1 and z_2 denote the bubble upstream and downstream stagnation points location

type vortex characterized by an upward stagnation circle located at the interface and a downward on-axis stagnation point as described in the previous section. This vortex pattern, according to the two corresponding bounding curves trend (Fig. 9), shrinks gradually with increasing until it utterly collapses and disappears at approximately $Re = 1070$ where the curves intersect. The single remaining curve over corresponds to the monotonic increase of the max interface level that leads to the bell shaped interface in a swirling flow that lacks breakdown.

4.1.5. Effect of sidewall differential rotation

4.1.5.1. Co-rotation

In this section, we investigate the response of the two-layer of immiscible rotating fluids to a modification of the background rotation by means of sidewall differential rotation. First, the flow driven by the cylindrical sidewall rotation alone is shown to exhibit a clockwise (anticlockwise) large meridian circulation above (below) the interface which, even at weak rotation rates, is sufficient to alter the flow vortex structure. This is best viewed with reference to Fig. 10 which illustrates the sidewall co-rotation applied to the reference flow state with still sidewall, driven by the lid rotation; namely ($S = 0$; $Re = 600$). It is remarked that weak co-rotation rates enhance vortex breakdown development in the more viscous fluid while relatively higher rates suppress the vortex structure, intensify the meridian circulation in the less viscous fluid and consequently strengthen interface shear and increase interface level. The case when both boundaries co-rotate with the same angular velocity, $S = 1$, led to a flow topology that lacks breakdown associated to a bell shaped thin interface layer, with significant axial elevationcompensated (for mass conservation) by a downward displacement adjacent to sidewall.

4.1.5.2. Counter-rotation

Low counter-rotation rates are shown to reduce sufficiently the angular momentum transfer from the rotating lid which causes a local swirl decay of the near axis helical core flow of the oil phase and consequently prevents VB occurrence. Besides, unlike the co-rotation counterpart, the swirling flow within and either side of the interface layer is entrained in the same radial inward direction with no apparent development of interface reverse flows as clearly depicted in Fig. 10, d, at the selected sidewall rotation rate ratio $S = -0.04$ and $Re = 1000$. Moreover, it is also remarked that the flow structure within the lower less viscous fluid is significantly altered and its direction reversed, as indicated by the anticlockwise bulk ambient motion associated to the development of a Moffatt type eddy at the lower disk-sidewall corner, typical of nonlinearcreeping flows at sharp angles.

The above findings were extended by exploring wider ranges of parameters which led to the establishment of the diagram of Fig. 11 which summarizes the sensitivity of the vortex flows development to the sidewall differential rotation over the selected ranges $500 < Re \leq 1000$ and $-0.04 \leq S \leq 0.16$. In particular, it identifies the regions of breakdown enhancement or suppression and provides the threshold bounding curve.
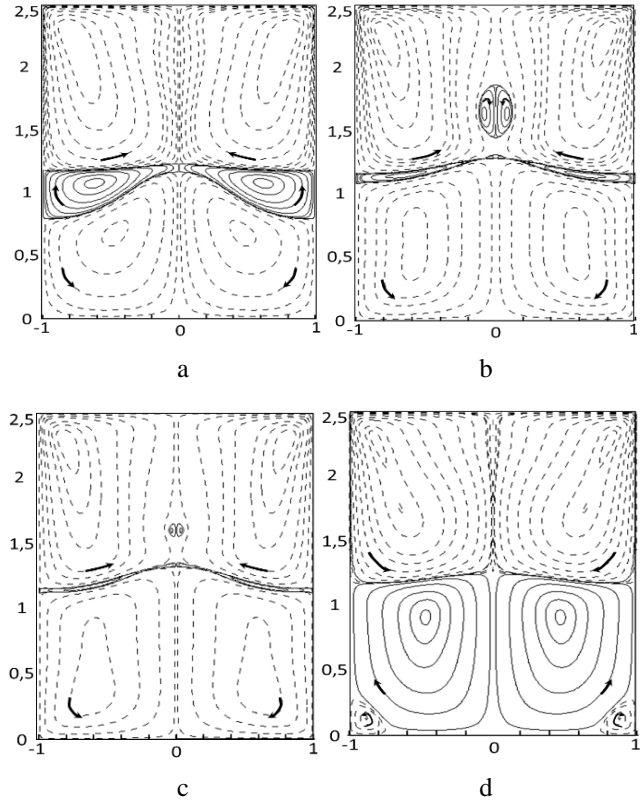

Fig. 10 Effect of sidewall co-rotation ($S > 0$) and counter-rotation ($S < 0$) on the lid driven flows at $Re = 600$ and $Re = 1000$ respectively: a – rotation of top only $S = 0$, b – co-rotation at $S = 0.008$, co-rotation at $S = 0.14$, d – counter-rotation at $S = -0.04$
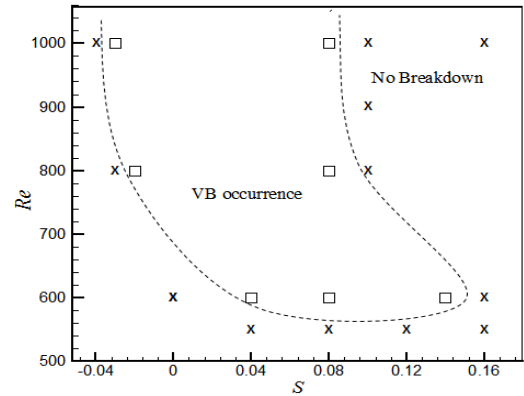

Fig. 11 Diagram mapping effects of sidewall co-rotation ($S > 0$) and counter-rotation ($S < 0$) on the development of VB in the upper fluid

4.2. Configuration with axial rod

In this section the configuration with an axial thin still/rotating rod is considered, aiming at investigating its impact on the vortex pattern of the lid driven two fluid system.

In the case of a still rod ($Re_r = 0$), the no slip conditions that apply at the cavity axis where found to slightly alter the stagnation flow conditions of breakdown onset as observed in prior experiments carried out on single fluids [21]. In particular, for the oil-glycerin configuration with rotating lid, the threshold Re for breakdown occurrence was found to depend upon the rod radius as depicted in Fig. 12 at three selected distinct volume fractions. It is
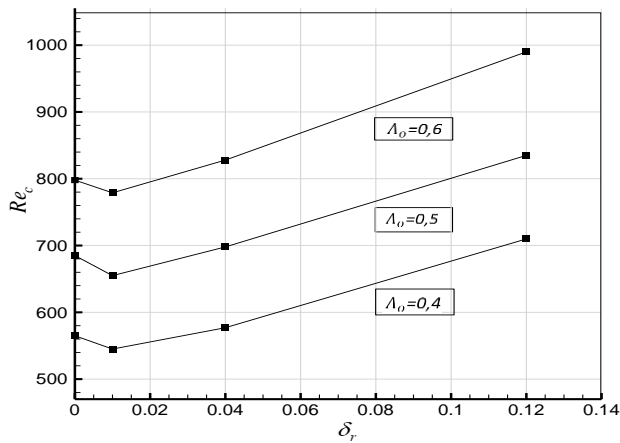
Fig. 12 Effect of a still rod radius ratio ($Re_r = 0$) on the threshold Re for breakdown onset in a two-fluid system for selected oil volume fraction
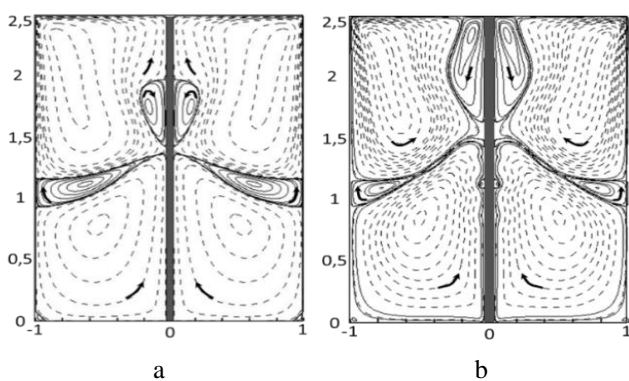

| a | b |

Fig. 13 Meridian pattern of a lid driven flow at $Re = 1000$: a – effect of a still rod $Re_r = 0$, b – effect of a co-rotating rod at $Re_r = 40.19$

remarked that over the selected rod radius range [0, 0.12], the corresponding three curves trends exhibit a local minimum with decreasing Re_c ($\approx 5\%$ reduction) over the approximate radius range [0, 0.01] before a steep increase at higher rod radii. Besides, the minimum Re_c, as expected, decreases with decreasing oil phase volume fraction.

When the rod is subjected to a moderate uniform rotation in the same direction as that of the lid (co-rotation), it generates a swirling co-flow (counter-flow) above (below) the interface that is revealed sufficiently strong to enhance breakdown expansion and interface elevation at the rod; commonly referred to as the rod climbing phenomenon, first observed by Bonn et al [14]. Further increase of the rod co-rotation rate led to the development of wavy streamlines pattern within the less viscous fluid associated to the onset of a Taylor type vortex cell at the rod-interface contact angle as illustrated in Fig. 13, b, at $Re = 1000$ and $Re_r = 40.19$, in comparison with the reference flow topology $Re_r = 0$ of Fig. 13, a, indicating the upper limit of the current investigation. This expected regime transition towards unsteadiness, attributed to the onset of a centrifugal instability, is consistent with experimental observations involving two-layer swirling flows of immiscible fluid [3, 14, 15]. Besides, the loss of the base flow stability and steadiness was also evidenced in the case of rod counter-rotation at much lower rotation rates ($\approx 60\%$ lower). Table 2 provides the numerically predicted threshold rod Reynolds number Re_r corresponding to five distinct lid rotational Reynolds number Re, at which Taylor like

vortex flows start to occur; including for comparison the case $Re = 0$ which refers to the cavity with still lid and rotating rod. A close value of Re_r is remarked over the Re range considered.

Table 2
Threshold Re_r for onset of Taylor vortices, at six Re values

Re	0	200	400	600	800	1000
Re_r	40.4	40.35	39.65	39.9	40.17	40.18

6. Conclusions

Swirling flows of an oil-glycerin system filling a cylinder of aspect ratio $\Lambda = 2.5$, with or without a central thin rod, are investigated numerically over the ranges of Reynolds number $500 \leq Re \leq 1100$ and oil volume fraction $0.2 \leq \Lambda_o \leq 0.8$.

For the flows driven by the rotating lid adjacent to the oil phase, in the absence of the rod, results revealed that:

1. At the threshold couple $(Re, \Lambda_o) \approx (510, 0.28)$ the helical core flow of the oil phase breaks; giving rise to the first on-axis bubble type breakdown. Above this critical point, breakdown onset was then identified over a bounded region of the (Re, Λ_o) space that widens with increasing $Re = 0$.

2. At the interface, as a result of the coupling effect of surface tension and shear, a thin anticlockwise cell emerges adjacent to the still sidewall while a large clockwise circulation drives the glycerin phase.

3. A decrease of the oil phase volume fraction Λ_o causes axial breakdown stretching, strengthens interface swirl and enhances interface elevation. Over the range $0.44 \leq \Lambda_o \leq 0.6$, at fixed Re, $800 \leq Re \leq 1100$, the bubble evolves into a ring type vortex which collapses onto the interface before it eventually disappears.

4. Flow stagnation may be prevented (enhanced) by means of low rates of sidewall counter-rotation (co-rotation) over the range $-0.04 \leq S < 0$ ($0 < S \leq 0.16$).

For the configuration with an axial rod, a near axis swirl induced by the rod differential rotation is found to favor breakdown onset and expansion, strengthen interface shear and causes interface rod climbing at low rotation rates. Relatively higher rates render the flow of the less viscous glycerin phase centrifugally unstable.

References

1. **Bonn, D.; Kobylko, M.; Bohn, S.; Meunier, J.; Morozov, A.; Van Saarloos, W.** 2004. Rod-climbing effect in Newtonian fluids, Physical Review Letters 93(21): 214503.
https://doi.org/10.1103/PhysRevLett.93.214503.
2. **Cunha, V. H. C.; Ribero, S. S.; Carvalho, M. S.** 2023. Breakup of thin liquid films with viscous interfaces, Physics of Fluids 35(7): 072101.
https://doi.org/10.1063/5.0153873.
3. **Liow, K. Y. S.; Tan, B. T.; Thouas, G. A.; Thompson, M. C.** 2009. CFD modeling of the steady-state momentum and oxygen transport in a bioreactor that is

driven by an aerial rotating disk, Modern Physics Letters B 23(02): 121-127.
https://doi.org/10.1142/S0217984909017893.

4. **Chai, X.; Dong, Y.; Qiu, F.; Li, W.; Zhang, L.; Cheng, Z.; Li, L.; Zhang, X.** 2024. Eddy Current Identification Methods and Applications in the Chemical Industry: A Mini-Review, ACS Omega 9(8): 8594-8600.
https://doi.org/10.1021/acsomega.3c09095.

5. **Zhao, C. W.; Gentric, C.; Dietrich, N.; Ma, Y. G.; Li, H. Z.** 2017. Deformation of liquid-liquid interfaces by a rotating rod, Physics of Fluids 29(7): 072108.
https://doi.org/10.1063/1.4995476.

6. **Lo Jacono, D.; Nazarinia, M.; Brøns, M.** 2009. Experimental vortex breakdown topology in a cylinder with a free surface, Physics of Fluids 21(11): 111704.
https://doi.org/10.1063/1.3265718.

7. **Brøns, M.; Voigt, L. K.; Sørensen, J. N.** 2001. Topology of vortex breakdown bubbles in a cylinder with a rotating bottom and a free surface, Journal of Fluid Mechanics 428: 133-148.
https://doi.org/10.1017/S0022112000002512.

8. **Herrada, M. A.; Shtern, V. N.; López-Herrera, J. M.** 2013. Off-axis vortex breakdown in a shallow whirlpool, Physical Review E 87(6): 063016.
https://doi.org/10.1103/PhysRevE.87.063016.

9. **Herrada, M.; Shtern, V.** 2014. Patterns of a creeping water-spout flow, Journal of Fluid Mechanics 744: 65-88.
https://doi.org/10.1017/jfm.2014.71.

10. **Fujimoto, S.; Takeda, Y.** 2009. Topology changes of the interface between two immiscible liquid layers by a rotating lid, Physical Review E 80(1): 015304.
https://doi.org/10.1103/PhysRevE.80.015304.

11. **Carrion, L.; Naumov, I. V.; Sharifullin, B. R.; Herrada, M. A.; Shtern, V. N.** 2020. Mechanism of Disappearance of Vortex Breakdown in a Confined Flow, Journal of Engineering Thermophysics 29(1): 49-66.
https://doi.org/10.1134/S1810232820010051.

12. **Brady, P. T.; Herrmann, M.; Lopez, J. M.** 2012. Two-fluid confined flow in a cylinder driven by a rotating end wall, Physical Review E 85(1): 016308.
https://doi.org/10.1103/PhysRevE.85.016308.

13. **Tsai, J. C.; Tao, C. Y.; Sun, Y. C.; Lai, C. Y.; Huang, K. H.; Juan, W. T.; Huang, J. R.** 2015. Vortex-induced morphology on a two-fluid interface and the transitions, Physical Review E 92(3): 031002.
https://doi.org/10.1103/PhysRevE.92.031002.

14. **Skripkin, S. G.; Sharifullin, B. R.; Naumov, I. V.; Shtern, V. N.** 2021. Dual vortex breakdown in a two-fluid whirlpool, Scientific Reports 11(1): 23085.
https://doi.org/10.1038/s41598-021-02514-6.

15. **Chandra, N. K.; Lahiri, K.; Kumar, A.** 2022. Contact angle hysteresis can modulate the Newtonian rod-climbing effect, Physics of Fluids 34(9): 093110.
https://doi.org/10.1063/5.0115521.

16. **Naumov, I. V.; Herrada, M. A.; Sharifullin, B. R.; Shtern, V. N.** 2018. Slip at the interface of a two-fluid swirling flow, Physics of Fluids 30(7): 074101.
https://doi.org/10.1063/1.5037222.

17. **Naumov, I. V.; Skripkin, S. G.; Kvon, A. Z.; Shtern, V. N.** 2023. Changing interface conditions in a two-fluid rotating flow, Physics of Fluids 35(6): 031705.
https://doi.org/10.1063/5.0141821.

18. **Bilger, C.; Aboukhedr, M.; Vogiatzaki, K.; Cant, R. S.** 2017. Evaluation of two-phase flow solvers using Level Set and Volume of Fluid methods, Journal of Computational Physics 345: 665-686.
https://doi.org/10.1016/j.jcp.2017.05.044.

19. **Fekhar, M.; Saci, R.; Gatignol, R.** 2021. Swirling flows characteristics in a cylinder under effect of buoyancy, Mechanika 27(3): 201-208.
https://doi.org/10.5755/j02.mech.27975.

K. Brahma, R. Saci, K. Mansouri, M. Imoula

FLOWS CHARACTERISTICS OF TWO IMMISCIBLE SWIRLING FLUIDS IN A CYLINDER

S u m m a r y

Flows of an oil-glycerin system of immiscible Newtonian fluids, driven by the independent rotation of the boundaries of a vertical cylinder with axial rod are investigated numerically. Moderate lid rotation rates are shown to generate breakdown in the adjacent oil phase, associated to significant interface displacement and flow reversal. The vortex pattern and interface behavior are found to be very sensitive to the distinct and combined effects of fluids volume fraction and background rotation. In particular, a decrease of the oil phase volume causes bubble expansion and evolution into a ring type vortex prior to its suppression as it coalesces onto a convex shaped interface. In addition, the vortex structure may efficiently be prevented (enhanced) by means of low rates of sidewall counter-rotation (co-rotation). Moreover, addition of swirl by means of the central rod rotation is found to have a considerable impact on the lid driven vortex flows characteristics in qualitative accord with prior experiments.